J. COMBIN. MATH. COMBIN. COMPUT. 127a (2025) 5031--5047

Journal of Combinatorial Mathematics and Combinatorial Computing
www.combinatorialpress.com/jcmcc

Combinatorial Press

Research on posture filtering algorithms for lower limb rehabilitation of patients with functional impairment in sports

Lei Wang[1, ✉]

[1] *Hunan Communications Vocational and Technical College, Changsha, Hunan, 410132, China*

ABSTRACT

This paper carries out a research on patients' lower limb posture capture strategy based on the lower limb rehabilitation of patients with sports function injury. The study is based on the posture filtering algorithm and designed a lower limb joint localization model based on the quaternion Kalman filter. The model utilizes five IMUs to capture the patient's lower limb movements to determine the posture of the patient's critical limbs in three-dimensional space and establish the joint coordinate system. Based on the filtered pose quaternions, the joint coordinate system of the lower limb is solved to obtain the optimal estimation of the lower limb pose. The results of simulation experiments show that the algorithm of this paper can make the motion data smoother and satisfy the motion requirements. The valuation of this paper's algorithm on the Z-axis in the single-axis rotation experiment is stable from -90° to 90°, while the valuation on the X-axis and Y-axis is near 0°. And the error in the ankle motion trajectory is small, with a mean value of 1.36°. The example results illustrate that the rehabilitation system equipped with the algorithm of this paper is basically consistent with the thigh elevation curve of the optical method in the patient's lower limb motion monitoring during walking, and the error is within 6°. The research in this paper provides a new technical means for lower limb rehabilitation training, which helps to improve the personalization and precision of rehabilitation training.

Keywords: Kalman filter; IMU; joint coordinate system; quaternion; lower limb rehabilitation exercise

1. Introduction

For a long time, the phenomena of low success rate, low athletic ability, and high incidence of injuries in Chinese youth sports athletes group have become one of the important factors restricting the development of Chinese sports reserves [1-2]. Throughout the world sports athletes injury situation can be found, mostly to the lower limbs, mainly for acute soft tissue injuries [3]. Compared with adult athletes, youth athletes as a group, their training methods and their corresponding common sports

✉ Corresponding author.
E-mail address: abc888guan@163.com (L. Wang).
Received 10 January 2024; Revised 15 February 2024; Accepted 25 December 2024; Published Online 15 April 2025.
DOI: 10.61091/jcmcc127a-284

injuries have their corresponding age characteristics, their bones, muscles, cardiorespiratory function, nervous system have their own developmental characteristics, and should not carry out excessive weight-bearing strength training and long-term maintenance of fixed posture training [4-6]. Adolescent athletes are easy to fatigue, and the elimination of fatigue is easy due to rapid anabolism. Adolescent sports athletes, once a sports injury occurs, should be dealt with in a timely and effective manner. Correct mastery of scientific training methods and injury occurrence laws to prevent and reduce the occurrence of injuries is of great significance in the development of youth sports in China [7-9].

Traditional lower limb rehabilitation training methods can only be carried out during hospitalization, while methods that require the assistance of a physical therapist require the therapist to have rich clinical experience and skilled rehabilitation training skills, so the therapist needs to invest a lot of time and energy to assist the patient in rehabilitation training, which will take up a lot of medical resources [10-12]. In addition, traditional rehabilitation training methods usually rely on the therapist's subjective assessment and the patient's self-feeling to assess the training effect, which is often difficult to objectively and accurately reflect the effect of rehabilitation training and the patient's recovery [13-14]. With the improvement of science and technology, modern rehabilitation training technology has been developed to a certain extent, through advanced rehabilitation equipment and technology, combined with computer and Internet technology, to realize the automation, personalization, and remoteness of rehabilitation training [15-16]. However, in China, the automation technology of rehabilitation training started late, and the system hardware cost for lower limb rehabilitation training is high, the system is complicated, and the system equipment needs professional technical support and maintenance. Therefore, how to carry out low-cost, high-efficiency, high-performance rehabilitation training methods is a current problem that needs to be solved [17-19].

Posture capture is a technique that utilizes sensor devices to track, observe, and record information about the motion of a critical limb in three-dimensional space. By capturing the body movement parameters of the subject, the true movement posture of the human body can be calculated and the information and parameters can be used to reconstruct, edit and analyze the human movement process [20-21]. The gesture capture technology has a wide range of application prospects and market space in multidisciplinary fields such as film and television production, human-computer interaction, virtual reality, fitness and sports training, and rehabilitation medicine. Among them, intelligent rehabilitation training systems based on posture capture technology have become a hot spot of attention in the field of rehabilitation medicine [22-23]. Commercially available posture capture and analysis systems have brought significant economic gains and social benefits to the field of rehabilitation medicine. With the scientific and refined development of rehabilitation medical care, these systems provide a tool for doctors to quantitatively analyze the changes in patients' conditions and rehabilitation, helping them to readily adjust the duration and intensity of patients' rehabilitation training, and to develop personalized rehabilitation treatment plans for patients [24-26].

The article analyzes the composition of posture during lower limb rehabilitation exercise based on motor anatomy, and introduces in detail the principle of capturing the patient's lower limb movement data using IMU, which serves as the data basis for subsequent research. A method based on the posture filtering algorithm for lower limb rehabilitation training of patients with sports function injuries is proposed. The method uses the quaternion-based Kalman filter model as a local filter. Based on the IMU to capture the patient's lower limb movement posture, establish the joint coordinate system, and solve the lower limb joint movement trajectory. Through simulation experiments, the effectiveness of the algorithm proposed in this paper is verified, and it is applied to a hospital to analyze the actual measurement effect of the algorithm.

2. Lower Extremity Rehabilitation Analysis and Lower Extremity Motion Data Acquisition

2.1. Lower Limb Rehabilitation Posture Study

The human lower extremity consists of three main joints: the hip, the knee and the ankle. According to motor anatomy, the hip has three degrees of freedom: flexion, extension, adduction, and rotation. The knee has two degrees of freedom: flexion, extension, and internal and external rotation. The ankle has two degrees of freedom: flexion and extension, and inversion and eversion. According to the three-dimensional coordinate plane defined by human anatomy, human motion can be analyzed in three datum planes: sagittal, horizontal and coronal planes. The main movement of the human lower limbs is concentrated in the sagittal plane, and the movement of the coronal plane and the horizontal plane is mainly to coordinate the balance of the lower limbs and turn and other prescribed actions.

Flexion and extension of the joints of the human lower limbs mainly refer to the hip, knee and ankle joints in the sagittal plane, while the joints of the lower limbs are adducted and retracted along the sagittal axis of the joints, and the joints of the lower limbs are internally rotated and externally rotated along the vertical axis of the joints, and finally the three joints of the lower limbs cooperate with each other to complete the regular movement of the human body.

The human lower limb consists of joints, lower limb bones and muscles, etc., and each joint is connected together by lower limb bones and muscles, and the normal walking process of human beings is realized through the joint cooperation of bones (including lower limb bones and joints), muscles and the related nervous system. In the process of lower limb movement, the lower limb bones are equivalent to the connecting rod, the joints are equivalent to the axis of rotation, the muscles provide the power, the nervous system to control, and ultimately realize the goal of movement. The human walking process is a cyclical movement process, in the process of walking, the feet alternately touch the ground, this process can be used gait to describe it. A complete gait cycle can be divided into two phases: the support phase and the swing phase, with the support phase accounting for about 60% of the entire walking cycle.

2.2. IMU-based Lower Limb Motion Data Acquisition

The IMU (Inertial Measurement Unit) [27] usually consists of a triaxial accelerometer, a triaxial gyroscope and/or a triaxial magnetometer. The triaxial accelerometer can capture the acceleration signals of the carrier in three orthogonal axes, and by processing the acceleration signals can get the static orientation information related to gravity, so as to calculate the inclination angle of the carrier when it is stationary, but it is susceptible to the influence of motion artifacts and bias. The three-axis gyroscope can capture the angular velocity signals of the carrier in three orthogonal axes, and through the integration of the angular velocity, the relative angle change of the carrier can be obtained, but the integration drift will occur with the accumulation of time. Through the geomagnetic field, the triaxial magnetometer is able to get the relative angle between the carrier and the geomagnetic field to confirm the direction, but the interference of the surrounding magnetic field has a greater effect on the output signal. Although in a specific environment, the individual sensor signals are prone to output biased data, but through the algorithm of the three sets of data for mutual fusion and compensation and other processing, can be obtained relatively more accurate information on the relative position of the carrier, attitude and joint angle. Kalman filtering and complementary filtering are the two most commonly used sensor fusion methods, in which Kalman filtering can obtain more accurate data but requires more computation, while complementary filtering requires less computation. The zero velocity update algorithm is one of the most commonly applied algorithms for correcting bias, which assumes that the foot is at rest during the gait support phase, when the linear and angular acceleration of the foot are defined as zero, and therefore the error due to integral drift can be reset. Typically, the output data is represented using quaternions, Euler angles or rotation matrices. The obtained data are transferred to the software paired with the IMU system and the kinematic data are computed by different anatomical calibration, fitting and data processing methods.

3. Kalman filter algorithm model

3.1. Equations of state and measurement equations

The state x to be estimated by the Kalman filter [28] is determined by the following linear stochastic difference equation:

$$x_k = Ax_{k\text{-}1} + Bu_{k\text{-}1} + w_{k\text{-}1} \tag{1}$$

where:

A is the state transfer matrix.

B is the association matrix of control input vector u with state vector x.

w is the process noise matrix.

The measurement equations are as follows:

$$z_k = Hx_k + v_k \tag{2}$$

where:

z is the measurement vector.

H is the association matrix of state vector x and measurement vector z.

v is the measurement noise matrix.

In the process and measurement equations, the process noise w and the measurement noise v are regarded as mutually independent white noises that satisfy the normal distribution, i.e:

$$p(w) \sim N(0, Q) \tag{3}$$

$$p(v) \sim N(0, R) \tag{4}$$

In practice, both the process noise covariance matrix Q and the measurement noise covariance matrix R vary with time and measurement moments, and are assumed to be constants here.

3.2. Kalman Filter Algorithm Flow

Kalman filtering uses feedback control to estimate a process: the filter estimates the state of the process at a given moment in time and adjusts this estimate with feedback from noisy measurements. The Kalman filter equation consists of two parts: the time update equation and the measurement update equation. The time update equation is responsible for predicting the current state and calculating the a priori estimated covariance. The measurement update equation is responsible for feedback control, i.e., combining the new measurements and the a priori estimate to obtain an improved a posteriori estimate. The time update equation can be viewed as a prediction process and the measurement update equation can be viewed as a correction process.

The time update equation consists of:

$$\begin{aligned} \hat{x}_k^- &= A\hat{x}_{k\text{-}1} + Bu_{k\text{-}1} \\ P_k^- &= AP_{k\text{-}1}A^T + Q \end{aligned} \tag{5}$$

These two equations predict the state and a priori covariance of the upcoming step k based on the state and covariance estimates of step $k-1$.

The state update equations include:

$$K = P_k^- H^T (HP_k^- H^T + R)^{-1} \tag{6}$$

$$\hat{x}_k = \hat{x}_{k\text{-}1} + K(z_k - H\hat{x}_{k\text{-}1}) \tag{7}$$

$$P_k = (I - KH)P_k^- \tag{8}$$

Figure 1 illustrates the complete Kalman filtering process. The first task of the state update equation is to compute the Kalman gain K, the next step is to obtain the a posteriori estimate based on the measurements z_k, and finally to compute the a posteriori estimate error covariance. Each time and measurement update uses the previous a posteriori estimate to predict this a priori estimate. This recursive property is a very attractive aspect of Kalman filtering because it makes the filter easier to implement.

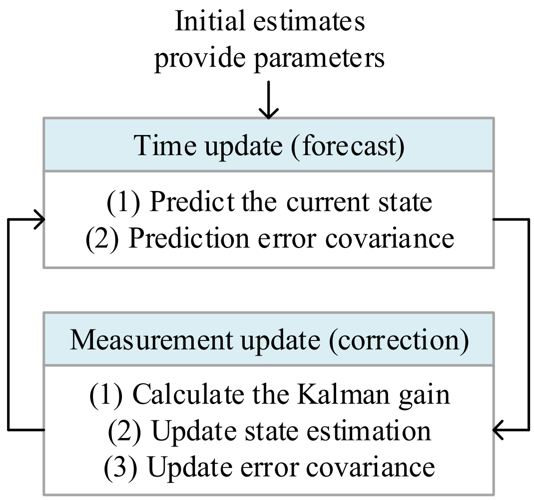

Fig. 1. Complete Kalman filtering process

3.3. Filter parameter selection

In the practical application of the Kalman filter, the measurement noise covariance R can be obtained in advance. This is because no matter how the process is measured, data containing the measurement noise is always available, and the measurement noise covariance R can be easily obtained from this data. The process noise covariance Q is not usually easy to obtain because there is no ability to be able to directly observe this process as hypothesized. But it is usually possible to obtain parameters R and Q experimentally.

In some cases where R and Q are constant, then the estimation error covariance P_k and Kalman gain K will stabilize quickly and remain constant, and these parameters can be derived in advance.

4. Lower limb joint localization method based on quaternion Kalman filter

4.1. Coordinate solution for lower limb kinematic joints

4.1.1. IMU Installation and Coordinate System Establishment. The motion state of the lower limb can be measured by five IMUs, which are fixed in the middle of the abdomen, thigh and calf of the human body. Among them, the IMU fixed in the thigh is responsible for acquiring the thigh posture, the IMU fixed in the calf is responsible for acquiring the calf posture, and the IMU in the fixed part is used as a reference point for the lower limb joint coordinate solution. The IMU fixed in the abdomen is immobilized with respect to the hip joint during the lower limb rehabilitation training. This IMU is mounted in the direction of X axis pointing directly above the body, Z axis pointing directly in front of the body, and O_XYZ conforming to the right-hand rule, which is regarded as the reference coordinate system (C system). The two IMUs fixed to the thigh and calf are mounted in the same direction, with X axes pointing downward parallel to the leg, Z axes pointing directly in front of the body, and O_XYZ conforming to the right-hand rule, which is regarded as the b system.

The joint coordinates are solved for the hip, knee and ankle joints [29]. Let the coordinate system of the hip joint be XYZ, the coordinate system of the knee joint be K_XYZ, and the coordinate system of the ankle joint be A_XYZ The direction of the coordinate system of the hip joint is the same as the direction of the C system, the direction of the joints and the ankle joints is the same as the direction of the b system, and the coordinate system is in the same plane as the O_XY plane of the C system.

4.1.2. Lower limb joint motion trajectory solution. As an example, the calculation of the right leg joint motion trajectory is described below:

The rotation matrix from the right knee joint coordinate system rotated to the C-system can be expressed as:

$$C_k^C = C_n^C C_k^n = C_n^C (C_n^k)^T \tag{9}$$

The rotation matrix from the right ankle to the C-system can be expressed as:

$$C_a^C = C_n^C C_a^n = C_n^C (C_n^a)^T \tag{10}$$

The coordinate position of the right hip joint in the C-system is known:

$$P_h = (x_h, y_h, z_h) \tag{11}$$

Since the X-axis of the knee coordinate system is parallel to the direction of the leg, only the knee joint in the X-axis direction has a component with respect to the reference point P_h. Then the coordinate position of the right knee joint in the C system is:

$$P_k = LpC_{k,1}^C + P_h \tag{12}$$

where $C_{k,1}^C$ denotes the first column vector of the coordinate transformation matrix C_k^c.

4.2. Lower Limb Joint Coordinate Solving for Observations

The known quaternion observation can be written as Q_k^l, where $l \in [1,5]$. k denotes the sampling point. $Q_k^1, Q_k^2, Q_k^3, Q_k^4, Q_k^5$ denotes the quaternion observations of the IMU fixed at the abdomen, right thigh, left thigh, right calf, and left calf, respectively. The rotation matrix from the right knee coordinate system to the C system is obtained and is represented by the following equation:

$$C_{keen_right,k}^C = C_{n,k}^C (C_{n,k}^{keen_right})^T \tag{13}$$

$$C_{n,k}^C = \begin{bmatrix} (q_{0,k}^1)^2 + (q_{1,k}^1)^2 - (q_{2,k}^1)^2 - (q_{3,k}^1)^2 & 2(q_{0,k}^1 q_{3,k}^1 + q_{1,k}^1 q_{2,k}^1) & 2(q_{1,k}^1 q_{3,k}^1 - q_{0,k}^1 q_{2,k}^1) \\ 2(q_{1,k}^1 q_{2,k}^1 - q_{0,k}^1 q_{3,k}^1) & (q_{0,k}^1)^2 - (q_{1,k}^1)^2 + (q_{2,k}^1)^2 - (q_{3,k}^1)^2 & 2(q_{0,k}^1 q_{3,k}^1 + q_{0,k}^1 q_{1,k}^1) \\ 2(q_{0,k}^1 q_{2,k}^1 + q_{1,k}^1 q_{3,k}^1) & 2(q_{2,k}^1 q_{3,k}^1 - q_{0,k}^1 q_{1,k}^1) & (q_{0,k}^1)^2 - (q_{1,k}^1)^2 - (q_{2,k}^1)^2 + (q_{3,k}^1)^2 \end{bmatrix} \tag{14}$$

$$C_{n,k}^{becen,ight} = \begin{bmatrix} (q_{0,k}^2)^2 + (q_{1,k}^2)^2 - (q_{2,k}^2)^2 - (q_{3,k}^2)^2 & 2(q_{0,k}^2 q_{3,k}^2 + q_{1,k}^2 q_{2,k}^2) & 2(q_{1,k}^2 q_{3,k}^2 - q_{0,k}^2 q_{2,k}^2) \\ 2(q_{1,k}^2 q_{2,k}^2 - q_{0,k}^2 q_{3,k}^2) & (q_{0,k}^2)^2 - (q_{1,k}^2)^2 + (q_{2,k}^2)^2 - (q_{3,k}^2)^2 & 2(q_{0,k}^2 q_{3,k}^2 + q_{0,k}^2 q_{1,k}^2) \\ 2(q_{0,k}^2 q_{2,k}^2 + q_{1,k}^2 q_{3,k}^2) & 2(q_{2,k}^2 q_{3,k}^2 - q_{0,k}^2 q_{1,k}^2) & (q_{0,k}^2)^2 - (q_{1,k}^2)^2 - (q_{2,k}^2)^2 + (q_{3,k}^2)^2 \end{bmatrix} \tag{15}$$

where $c_{keen\_right,k}^c$ denotes the rotation matrix from the right knee coordinate system to the C system at the k moment. $C_{n,k}^C$ denotes the rotation matrix from the n-system to the C-system at the k-moment. $C_{n,k}^{keen\_right}$ denotes the rotation matrix of the n system to the right knee joint coordinate system at the moment k.

The rotation matrix from the right ankle joint coordinate system to the C system is obtained and is expressed by the following equation:

$$C_{ankle_right,k}^{C}=C_{n,k}^{C}(C_{n,k}^{ankle_right})^{T} \tag{16}$$

$$C_{n,k}^{ankle}=\begin{bmatrix}(q_{0,k}^{4})^{2}+(q_{1,k}^{4})^{2}-(q_{2,k}^{4})^{2}-(q_{3,k}^{4})^{2} & 2(q_{0,k}^{4}q_{3,k}^{4}+q_{1,k}^{4}q_{2,k}^{4}) & 2(q_{1,k}^{4}q_{3,k}^{4}-q_{0,k}^{4}q_{2,k}^{4})\\ 2(q_{1,k}^{4}q_{2,k}^{4}-q_{0,k}^{4}q_{3,k}^{4}) & (q_{0,k}^{4})^{2}-(q_{1,k}^{4})^{2}+(q_{2,k}^{4})^{2}-(q_{3,k}^{4})^{2} & 2(q_{0,k}^{4}q_{3,k}^{4}+q_{0,k}^{4}q_{1,k}^{4})\\ 2(q_{0,k}^{4}q_{2,k}^{4}+q_{1,k}^{4}q_{3,k}^{4}) & 2(q_{2,k}^{4}q_{3,k}^{4}-q_{0,k}^{4}q_{1,k}^{4}) & (q_{0,k}^{4})^{2}-(q_{1,k}^{4})^{2}-(q_{2,k}^{4})^{2}+(q_{3,k}^{4})^{2}\end{bmatrix} \tag{17}$$

where $C_{ankle\_right.k}^{c}$ denotes the rotation matrix from the right ankle coordinate system to the C-system at moment k. $C_{n,k}^{ankle\_right}$ denotes the rotation matrix from the n system to the right ankle coordinate system at the moment of k.

Similarly, the rotation matrix of the left knee coordinate system to the C system is obtained with and the rotation matrix of the left ankle coordinate system to the C system is as follows:

$$C_{keen\_left,k}^{C}=C_{n,k}^{C}(C_{n,k}^{keen\_left})^{T} \tag{18}$$

$$C_{n,k}^{kown}=\begin{bmatrix}(q_{0,k}^{3})^{2}+(q_{1,k}^{3})^{2}-(q_{2,k}^{3})^{2}-(q_{3,k}^{3})^{2} & 2(q_{0,k}^{3}q_{3,k}^{3}+q_{1,k}^{3}q_{2,k}^{3}) & 2(q_{1,k}^{3}q_{3,k}^{3}-q_{0,k}^{3}q_{2,k}^{3})\\ 2(q_{1,k}^{3}q_{2,k}^{3}-q_{0,k}^{3}q_{3,k}^{3}) & (q_{0,k}^{3})^{2}-(q_{1,k}^{3})^{2}+(q_{2,k}^{3})^{2}-(q_{3,k}^{3})^{2} & 2(q_{0,k}^{3}q_{3,k}^{3}+q_{0,k}^{3}q_{1,k}^{3})\\ 2(q_{0,k}^{3}q_{2,k}^{3}+q_{1,k}^{3}q_{3,k}^{3}) & 2(q_{2,k}^{3}q_{3,k}^{3}-q_{0,k}^{3}q_{1,k}^{3}) & (q_{0,k}^{3})^{2}-(q_{1,k}^{3})^{2}-(q_{2,k}^{3})^{2}+(q_{3,k}^{3})^{2}\end{bmatrix} \tag{19}$$

$$C_{ankle_left,k}^{C}=C_{n,k}^{C}(C_{n,k}^{ankle_left})^{T} \tag{20}$$

$$C_{n,k}^{ankk-kqt}=\begin{bmatrix}(q_{0,k}^{s})^{2}+(q_{1,k}^{s})^{2}-(q_{2,k}^{s})^{2}-(q_{3,k}^{s})^{2} & 2(q_{0,k}^{s}q_{3,k}^{s}+q_{1,k}^{s}q_{2,k}^{s}) & 2(q_{1,k}^{s}q_{3,k}^{s}-q_{0,k}^{s}q_{2,k}^{s})\\ 2(q_{1,k}^{s}q_{2,k}^{s}-q_{0,k}^{s}q_{3,k}^{s}) & (q_{0,k}^{s})^{2}-(q_{1,k}^{s})^{2}+(q_{2,k}^{s})^{2}-(q_{3,k}^{s}) & 2(q_{0,k}^{s}q_{3,k}^{s}+q_{0,k}^{s}q_{1,k}^{s})\\ 2(q_{0,k}^{s}q_{2,k}^{s}+q_{1,k}^{s}q_{3,k}^{s}) & 2(q_{2,k}^{s}q_{3,k}^{s}-q_{0,k}^{s}q_{1,k}^{s}) & (q_{0,k}^{s})^{2}-(q_{1,k}^{s})^{2}-(q_{2,k}^{s})^{2}+(q_{3,k}^{s})^{2}\end{bmatrix} \tag{21}$$

where $C_{keen\_leff,k}^{C}$ denotes the rotation matrix from the left knee coordinate system to the C system at the k moment. $C_{n,k}^{keen\_left}$ denotes the rotation matrix from the n-system to the left knee joint at the k-moment. $C_{ankle\_leff,k}^{C}$ denotes the rotation matrix from the left ankle coordinate system to the C system at the k moment. $C_{n,k}^{ankle\_left}$ represents the rotation matrix from the n system to the left ankle joint at the k th moment.

It is known that the coordinates of the left and right hip joints relative to the reference point are respectively:

$$P_{hip_right}=(x_{hip_right},y_{hip_right},z_{hip_right}) \tag{22}$$

$$P_{hip_left}=(x_{hip_left},y_{hip_left},z_{hip_left}) \tag{23}$$

The right knee, right ankle, left knee and left ankle coordinates are expressed in the following equation:

$$P_{keen_right,k}=L_{P}C_{keen_right,kll}^{C}+P_{hip_right} \tag{24}$$

$$P_{ankle_right,k}=Ld\,C_{ankle_right,kll}^{C}+P_{keen_right,k} \tag{25}$$

$$P_{keen_left,k}=Lp\,C_{keen_left,k|1}^{C}+P_{hip_left} \tag{26}$$

$$P_{ankle_left,k}=Ld\,C_{ankle_left,kl1}^{C}+P_{keen_left,k} \tag{27}$$

where $P_{keen\_right,k},P_{ankle\_right,k},P_{keen\_left,k},P_{ankle\_leff,k}$ denotes the right knee, right ankle, left knee, and left ankle coordinates in order at moment k. $C_{keen\_right,kll}^{C},C_{ankle\_right,kll}^{C},C_{keen\_leff,kll}^{C},C_{ankle\_leff,kll}^{C}$ denotes the first column of the corresponding rotation matrix.

4.3. Quaternion Kalman Filter Lower Limb Joint Coordinate Solution

4.3.1. Quaternion-based Kalman Filter Modeling. The Quaternion-based Kalman Filter (QKF) model is shown in Fig. 2. In this model, the QKF filtering process is first performed on the data collected from the five IMUs fixed in the abdomen, thigh and calf parts respectively, and then the filtering results are used to solve the lower limb joint positions to obtain the accurate lower limb joint coordinates. Where QKF takes quaternions as state vectors, the recurrence relation of quaternions is realized by using the quaternion differential equation [30], so as to establish the state equation of QKF. It is known that the IMU output data include quaternion number, angular velocity, etc., and the observation equation with quaternion number as the observation vector is established according to the relationship between the state vector and the observation output.

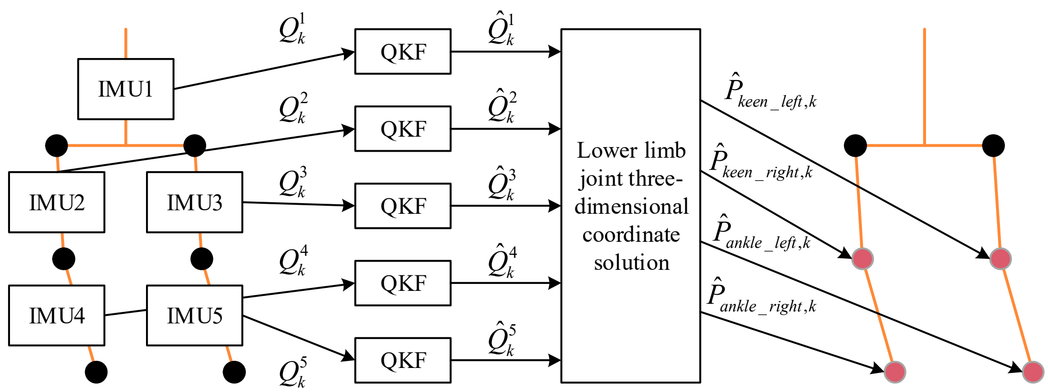

Fig. 2. Kalman filter model based on quaternion

The equation of state of the QKF can be written as equation (28):

$$\underbrace{\begin{bmatrix} q'_{1,k} \\ q'_{2,k} \\ q'_{3,k} \\ q'_{4,k} \end{bmatrix}}_{Q_k^l} = \underbrace{\begin{bmatrix} 1 & -\frac{1}{2}\omega'_{x,k-1}T & -\frac{1}{2}\omega'_{y,k-1}T & -\frac{1}{2}\omega'_{z,k-1}T \\ \frac{1}{2}\omega'_{x,k-1}T & 1 & \frac{1}{2}\omega'_{z,k-1}T & -\frac{1}{2}\omega'_{y,k-1}T \\ \frac{1}{2}\omega'_{y,k-1}T & -\frac{1}{2}\omega'_{z,k-1}T & 1 & \frac{1}{2}\omega'_{x,k-1}T \\ \frac{1}{2}\omega'_{z,k-1}T & \frac{1}{2}\omega'_{y,k-1}T & -\frac{1}{2}\omega'_{x,k-1}T & 1 \end{bmatrix}}_{F_{k-1}^l} \underbrace{\begin{bmatrix} q'_{1,k-1} \\ q'_{2,k-1} \\ q'_{3,k-1} \\ q'_{4,k-1} \end{bmatrix}}_{F'_{k-1}} + w'_{k-1} \tag{28}$$

where Q_k^l denotes the state vector of the lnd sensor under the time index k, i.e., the attitude quaternion. F_k^l denotes the state transfer matrix, which consists of the sampling period T and the angular velocity $\left[\omega_{x,k}^l, \omega_{y,k}^l, \omega_{z,k}^l\right]^T$, and w_k^l denotes the process noise, which obeys a Gaussian distribution $w_k^l \sim N(0, M^l)$.

The observation equation of QKF:

$$\underbrace{\begin{bmatrix} \hat{q}_{1,k}^l \\ \hat{q}_{2,k}^l \\ \hat{q}_{3,k}^l \\ \hat{q}_{4,k}^l \end{bmatrix}}_{Z_k^l} = \underbrace{\begin{bmatrix} 1 & 0 & 0 & 0 \\ 0 & 1 & 0 & 0 \\ 0 & 0 & 1 & 0 \\ 0 & 0 & 0 & 1 \end{bmatrix}}_{H^l} \underbrace{\begin{bmatrix} q_{1,k}^l \\ q_{2,k}^l \\ q_{3,k}^l \\ q_{4,k}^l \end{bmatrix}}_{Q_k^l} + \gamma_k^l \tag{29}$$

where Z_k^l denotes the observation vector of the l nd sensor at time index k, i.e., the attitude quaternion observation. H^l denotes the observation matrix, i.e., the 4th order unit matrix. γ_k^l denotes the observation noise, which obeys a Gaussian distribution $\gamma_k^l \sim \mathrm{N}\,(0, N^l)$.

Therefore, the QKF can be written as Eq:

$$\begin{cases} Q_k^l = F_{k-1}^l Q_{k-1}^l + w_{k-1}^l \\ Z_k^l = H^l Q_k^l + \gamma_k^l \end{cases} \tag{30}$$

For all five IMUs in this model, the filters of the above equation are used. If the initial value Q_0^l and the value of angular velocity at each moment are known for each filter state vector, the steps of the algorithm implementation are as follows:

State one-step prediction:

$$\hat{Q}_{k|k-1}^l = F_{k-1}^l \hat{Q}_{k-1}^l \tag{31}$$

One-step prediction of the attitude quaternion at moment k using the estimated attitude quaternion $\hat{Q}_{k-1}^l$ at moment $(k-1)$ with one-step prediction $\hat{Q}_{k1k-1}^l$.

State Error Skewed Variance Prediction:

$$P_{k|k-1}^l = F_{k-1}^l P_{k|k-1}^l (F_{k-1}^l)^T + M^l \tag{32}$$

where $P_{k|k-1}^i$ denotes the predicted value of the state-volume error covariance.

Kalman gain calculation:

$$K_k^l = P_{k|k-1}^l (H^l)^T [N^l + H^l P_{k|k-1}^l (H^l)^T]^{-1} \tag{33}$$

where K_k^i is denoted as the Kalman gain coefficient, which fuses the measured and state quantities in one step to the predicted value, and can be weighed against the magnitude of the predicted covariance and the observed covariance depending on the size of K_k^i.

State Estimation:

$$\hat{Q}_k^l = \hat{Q}_{k|k-1}^l + K_k^l \left[Z_k^l \cdot H^l \hat{Q}_{k|k-1}^l \right] \tag{34}$$

State estimation fuses the one-step predicted value $\hat{Q}_{kk-1}^l$ and the observed value Z_k^l of the state, and achieves the optimal estimation of the state quantity through the trade-off effect of the Kalman gain K_k^l.

State error covariance estimation:

$$P_k^i = \left[I - K_k^i H^i \right] P_{k|k-1}^i \tag{35}$$

Finally, the state error covariance needs to be updated for the calculation of the Kalman gain K_{k+1}^l at the next moment.

4.3.2. Lower Limb Joint Coordinate Solving. After realizing the optimal estimation of the quaternion, then combining the relative reference point coordinates of the hip joint $P_{hip\_right}, P_{hip\_left}$ and the limb length Lp, Ld, the solution of the lower limb joint coordinates is realized, and its solution process is consistent with that of the lower limb joint coordinates based on the observation value. The lower limb joint coordinate solving process is shown in Fig. 3.

Where $\hat{Q}_k^l$ denotes the quaternion after QKF filtering. $\hat{C}$ denotes the rotation matrix solved using $\hat{Q}_k^l$. $\hat{P}$ represents the result of joint coordinate solving after filtering.

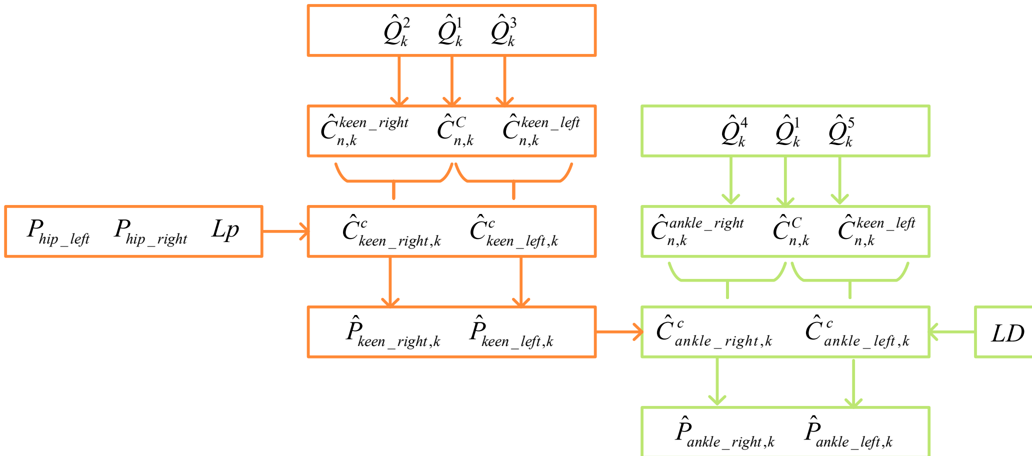

Fig. 3. Process of solving three-dimensional coordinate of lower limb joint

4.4. Simulation experiment and practical application analysis

4.4.1. Analysis of the effect of filtering and prediction of lower limb movement data. The experiments in this section focus on verifying the filtering as well as prediction effects of the quaternion-based Kalman filter in data processing. The experimental steps are as follows:

1) The data collected by the IMU is processed directly.

2) The collected data are Kalman filtered and then processed in the same way. Finally, the two kinds of data were compared.

Two main experiments were designed for the ankle and knee joints respectively: experiment 1, the main movement for the ankle joint, in which the experimenter wore the IMU, perpendicular to the torso, and rotated on the axis of the ankle joint at normal speed. Experiment 2, the main movement of the knee joint, sitting on a chair, feet flat on the ground, slowly raise one leg to, and then slowly lower, alternating legs.

The raw coordinate data collected in the IMU, input into MATLAB, one kind of direct motion state transformation, one kind of filtering processing, and then motion state transformation. Finally, the key skeletal point information of the lower limb was extracted from the two kinds of data, which was processed by MATLAB to display the motion trajectory and construct the mathematical model.

Figure 4 demonstrates the abduction/adduction of the ankle joint, the anterior flexion/posterior extension of the knee joint and the motion information. As can be seen from the figure, the data processed by the algorithm of this paper is relatively earlier than the original data, which can effectively improve the lag caused by the information acquisition process. When the ankle or knee joint movement is performed, it will not be strictly parallel to the human torso, so the movement angle will not tend to 0, as shown in the figure, it is about 10°. The other movement inflection points in the three diagrams, for the movement transition moments, can be seen through the Kalman filtered data changes are more smooth and gentle, more to meet the needs of the movement.

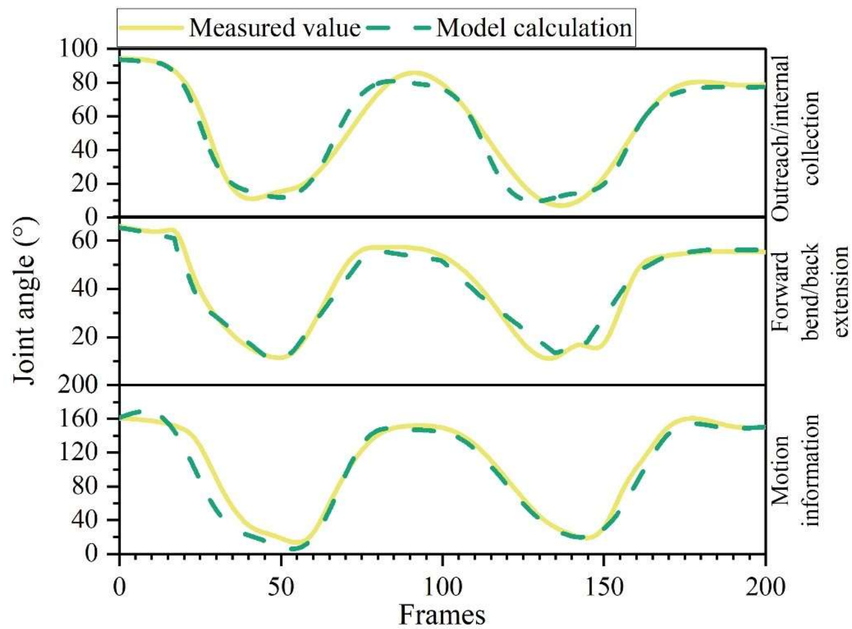

Fig. 4. The motion information of the ankle joint knee

4.4.2. Filter robustness detection based on uniaxial rotation. The attitude estimation experiment of IMU generally uses a three-degree-of-freedom rotary table, firstly, the IMU is mounted on the rotary table, and the rotary table is allowed to rotate according to the known attitude trajectory, and then the attitude trajectory of IMU is solved by the designed attitude estimation algorithm of IMU, and the convergence and accuracy of the attitude estimation algorithm can be verified by comparing the solved attitude estimation with the rotary table-turned attitude trajectory.

In this section, a single-axis rotation experiment of the IMU is designed, in which one ruler of the long ruler protractor is fixed on the tabletop with transparent tape so that the other ruler can rotate freely. One side of the IMU module is fastened to the rod of the movable ruler so that the Z-axis of the IMU coordinate system is perpendicular to the ruler surface, and the rotation of the rod of the movable ruler can drive the IMU to rotate around its Z-axis. So that the scale of the movable ruler on the protractor changes back and forth between 0º and 180º, the results of the uniaxial experimental algorithm angle estimation are shown in Figure 5. From the figure, it can be seen that: the lower limb joint localization method based on quaternion Kalman filter designed in this paper has high estimation accuracy. The estimation value in the Z-axis direction basically varies back and forth between -90° and 90°. And the estimation accuracy in the Y-axis and X-axis is basically the same, both floating up and down in the 0° angle. The experimental results show that the method in this paper has high filtering accuracy and robustness, and can meet the posture estimation and localization research on the rehabilitation of patients with lower limb injury.

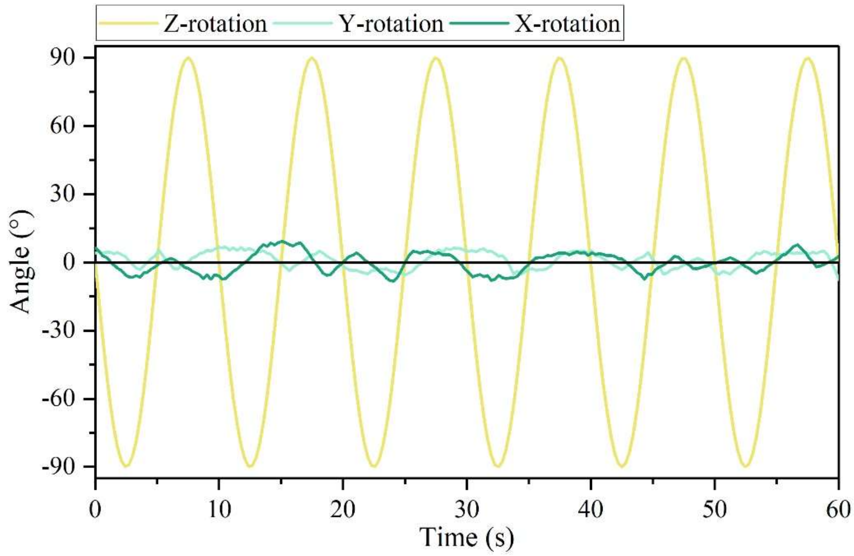

Fig. 5. An estimate of the Angle of single spindle rotation experiment

4.4.3. Evaluation of the effect of visual driving of human motion trajectories. The lower limb joint localization model proposed in this paper is used to conduct on-line experiments with the rehabilitation system, and the human lower limb joint angles output by the IMU are compared with the actual movement angles and trajectories of the rehabilitation robot. The participant performs the pre-designed rehabilitation training movements through the IMU, and the joint data are collected by the IMU, processed by the program of the host computer and written into the cached data file, which is then read by the control program of the host computer, and the lower limb rehabilitation system is controlled based on the data file. The rehabilitation system incorporating the algorithm of this paper can follow the lower limb movement of the tested experimenter better in the experiment, and the output real angle trajectory of the ankle joint is compared with the movement angle trajectory of the rehabilitation system.

The ankle data were collected as input, and the results of the comparison of the visual driving effect of the motion trajectory are shown in Fig. 6, and Fig. 7 shows the error between the output of this paper's model and the real motion angle. The dotted line in Fig. 6 is the joint mobility data acquired by the rehabilitation system equipped with this paper's algorithm, and the solid line is the output of the real motion angle data. Combining the two figures and analyzing the experimental data processing, the average value of the error between the two signals in the descending and ascending segments is 1.36°, and the maximum point of the error occurs at the wave valley and wave peak, which is up to 4.91°. This may be in the trough and crest will be affected by the load change and the actuator commutation, while the data acquisition of the IMU has nothing to do with the mechanical structure, so the two curves are less similar in the crest, but the output curve of the rehabilitation system equipped with the model of this paper is more similar to the human body movement trajectory.

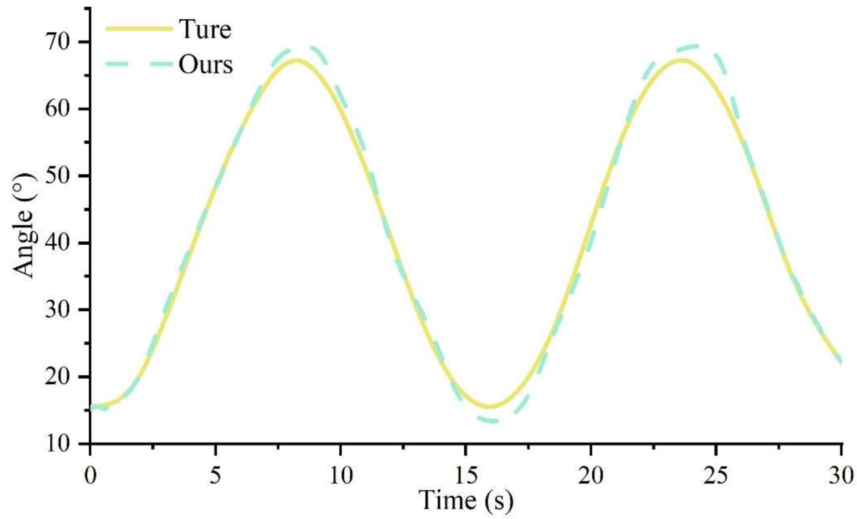

Fig. 6. Visual drive effect comparison results

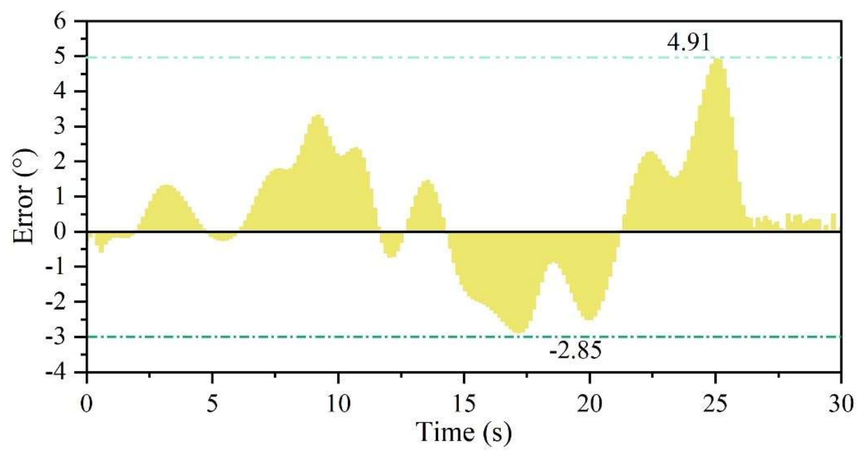

Fig. 7. Error between model output and real motion Angle in this paper

4.4.4. Evaluation of the Effectiveness of Practical Application of Rehabilitation Training. The algorithm of this study was applied to the rehabilitation department of a hospital for disciplinary research. The selection of cases is based on two main points: patients need to have good motor ability and perform large movements during the monitoring process. The patient should have good compliance and cognitive ability to wear the device for a long time to complete the monitoring. Based on the above considerations, five home rehabilitation patients with normal cognitive ability were selected for the initial experiments in this study.

After the algorithm in this paper was deployed at the patients' home, each patient wore the sensor for 1h of motion capture in the morning and afternoon. During the experiment, the patients performed a total of 30 min of rehabilitation training according to the doctor's request, which included 10 min of treadmill walking training, and the rest of the time was free to move around indoors, and the experiment lasted for 6 weeks. In order to ensure the reproducibility of the experiment, the walking training with high similarity was selected for the test, and the treadmill speed was set at 2km/h when the patient was walking.In addition, the experiment used the optical tracking method as a reference to synchronously record the walking video at a frame rate of 25Hz. The angle between the midline of the thigh and the vertical direction was measured frame by frame on the resulting video to form the pitch angle curve.

Figures 8 and 9 show the thigh pitch angle curves and errors during walking, respectively. Combining the two figures, it can be seen that the two curves show the same trend of change, and the maximum deviation of the thigh pitch angle monitored by the two methods is 0.093 radians (≈5.30°), the minimum deviation is close to 0 radians, and the average difference is 0.024 radians (≈1.37°). The TD in the figure represents the time difference between the optical method and the Kalman filter algorithm in tracking the limb to reach a certain angular peak (at the maximum thigh pitch angle), because the optical method is a real-time, frame-by-frame measurement with a maximum latency of only 40 ms (25 Hz frame rate), the TD characterizes the latency of the device. The TD in the figure is 1.8s, and the increase of the delay is related to the algorithm of this paper, which may be the model of this paper, when there is a sudden change of the angular velocity, such as in the example of the swing speed of the thigh is suddenly increased or decreased, the value of the angular velocity and the corresponding covariance matrix need to go through a few iterations in order to match the current motion, which is represented as a lag time on the filtering results.

The evaluation of the use of the system by the rehabilitation doctor is also used as part of the experiment, where the rehabilitation doctor faces the patient and observes the actual movements and the model movements displayed by the mobile terminal using the algorithm of this paper, and the evaluation concludes that: the model movements are well reproduced with respect to the patient's actual movements, and the movements are accurate and continuous, which can be used instead of manual monitoring, and does not use a camera and does not infringe on the patient's privacy. The joint mobility of the movement is within 6° from the manual measurement, which meets the needs of rehabilitation medicine for motor function assessment and training guidance. Equipped with a quadratic Kalman filter algorithm, the sensor delay is within 2s, with good real-time, unexpected events can be quickly responded to, to ensure the safety of the patient's out-of-hospital rehabilitation.

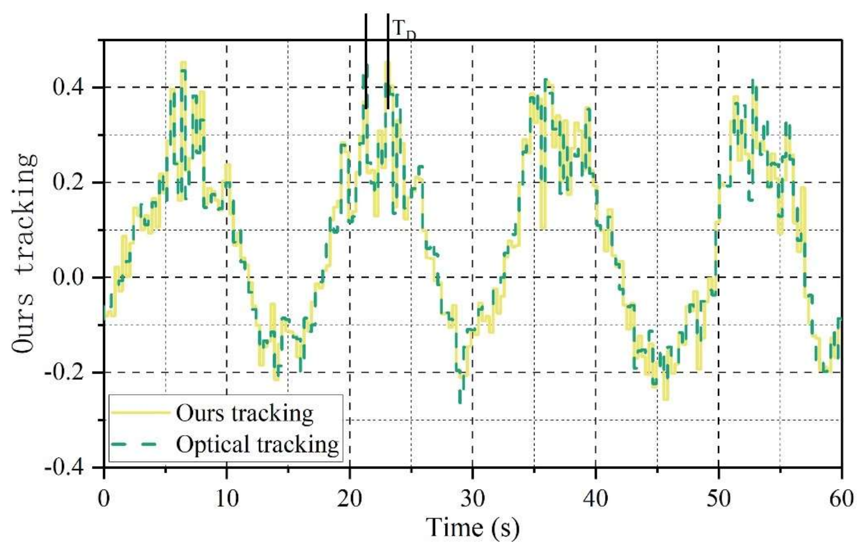

Fig. 8. The stroke of the leg of the walking process

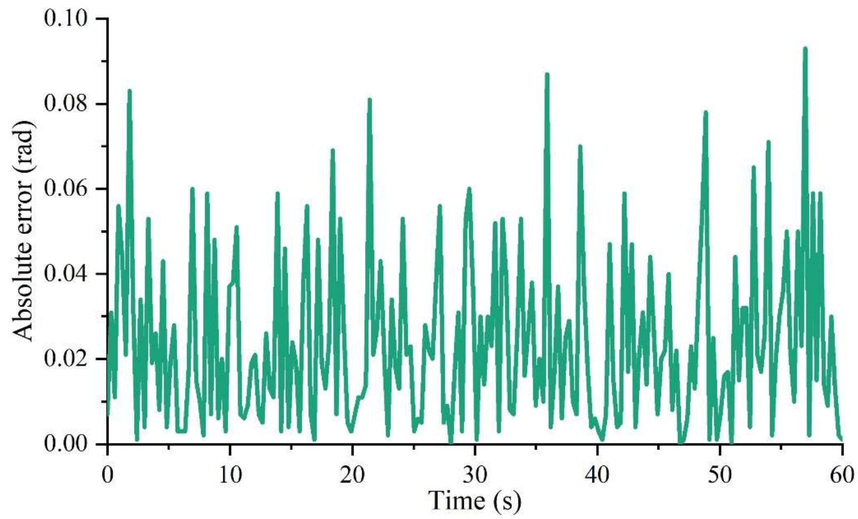

Fig. 9. The Angle error of big leg in the walking process

5. Conclusion

In the course of this research, gait data from patients with sports function injuries were collected, and based on the data characteristics, a lower limb joint localization model based on a quaternion Kalman filter is proposed. The model can dynamically adjust the filter parameters according to the real-time data of lower limb posture captured by the IMU to improve the filtering accuracy and robustness. The coordinates of the lower limb joints are solved by establishing the state equation of the QKF and the observation equation with quaternions as observation vectors, and finally the accurate localization of the lower limb joints is completed.

The motion data of abduction/adduction of ankle joint and forward flexion/backward extension of knee joint under the algorithm of this paper reach the inflection point faster than the original data. And the estimation value on the Z-axis rotation changes regularly from -90° to 90°, while the estimation accuracy on the X-axis and Y-axis is also higher. The maximum relative errors of the ankle trajectory are at the trough (-2.85°) and the peak (4.91°), and the overall output curve is consistent with the human trajectory. And the rehabilitation doctor evaluates the rehabilitation system under this paper's algorithm highly, and it has a better effect of motion monitoring on patients with lower limb injuries. In conclusion, applying the algorithm of this paper to rehabilitation training has important practical value for promoting the recovery of patients' motor function.

Funding

This research was supported by the research project of Education and Teaching Reform in Vocational Colleges in Hunan Province: Research on the Construction of "Liang Xing Yi Du" Golden Course Curriculum System of Fitness Qigong in Universities under the Background of Digital China Construction (ZJGB2022236).

About the Author

Lei Wang, (1985-02), male, Han Nationality, Yongzhou, Hunan province, master, lecturer, research direction of ethnic traditional sports.

References

[1] Soligard, T., Steffen, K., Palmer, D., Alonso, J. M., Bahr, R., Lopes, A. D., ... & Engebretsen, L. (2017). Sports

injury and illness incidence in the Rio de Janeiro 2016 Olympic summer games: a prospective study of 11274 athletes from 207 countries. British journal of sports medicine, 51(17), 1265-1271.

[2] Soligard, T., Palmer, D., Steffen, K., Lopes, A. D., Grant, M. E., Kim, D., ... & Engebretsen, L. (2019). Sports injury and illness incidence in the PyeongChang 2018 Olympic winter games: a prospective study of 2914 athletes from 92 countries. British Journal of Sports Medicine, 53(17), 1085-1092.

[3] Patel, D. R., Yamasaki, A., & Brown, K. (2017). Epidemiology of sports-related musculoskeletal injuries in young athletes in United States. Translational pediatrics, 6(3), 160.

[4] Timpka, T., Janson, S., Jacobsson, J., Dahlström, Ö., Spreco, A., Kowalski, J., ... & Svedin, C. G. (2019). Lifetime history of sexual and physical abuse among competitive athletics (track and field) athletes: cross sectional study of associations with sports and non-sports injury. British journal of sports medicine, 53(22), 1412-1417.

[5] Lin, C. Y., Casey, E., Herman, D. C., Katz, N., & Tenforde, A. S. (2018). Sex differences in common sports injuries. PM&R, 10(10), 1073-1082.

[6] Prieto-González, P., Martínez-Castillo, J. L., Fernández-Galván, L. M., Casado, A., Soporki, S., & Sánchez-Infante, J. (2021). Epidemiology of sports-related injuries and associated risk factors in adolescent athletes: an injury surveillance. International journal of environmental research and public health, 18(9), 4857.

[7] Bolling, C., Delfino Barboza, S., van Mechelen, W., & Pasman, H. R. (2019). How elite athletes, coaches, and physiotherapists perceive a sports injury. Translational Sports Medicine, 2(1), 17-23.

[8] Jauhiainen, S., Kauppi, J. P., Leppänen, M., Pasanen, K., Parkkari, J., Vasankari, T., ... & Äyrämö, S. (2021). New machine learning approach for detection of injury risk factors in young team sport athletes. International journal of sports medicine, 42(02), 175-182.

[9] Dhillon, H., Dhilllon, S., & Dhillon, M. S. (2017). Current concepts in sports injury rehabilitation. Indian journal of orthopaedics, 51(5), 529-536.

[10] Shi, D., Zhang, W., Zhang, W., & Ding, X. (2019). A review on lower limb rehabilitation exoskeleton robots. Chinese Journal of Mechanical Engineering, 32(1), 1-11.

[11] Zhou, J., Yang, S., & Xue, Q. (2021). Lower limb rehabilitation exoskeleton robot: A review. Advances in Mechanical Engineering, 13(4), 16878140211011862.

[12] Higashimoto, Y., Ando, M., Sano, A., Saeki, S., Nishikawa, Y., Fukuda, K., & Tohda, Y. (2020). Effect of pulmonary rehabilitation programs including lower limb endurance training on dyspnea in stable COPD: A systematic review and meta-analysis. Respiratory investigation, 58(5), 355-366.

[13] Zou, Y., Wang, N., Wang, X., Ma, H., & Liu, K. (2018). Design and experimental research of movable cable-driven lower limb rehabilitation robot. IEEE Access, 7, 2315-2326.

[14] Zhou, J., Li, Z., Li, X., Wang, X., & Song, R. (2021). Human–robot cooperation control based on trajectory deformation algorithm for a lower limb rehabilitation robot. IEEE/ASME Transactions on Mechatronics, 26(6), 3128-3138.

[15] Yu, F., Liu, Y., Wu, Z., Tan, M., & Yu, J. (2024). Adaptive Gait Training of a Lower Limb Rehabilitation Robot Based on Human–Robot Interaction Force Measurement. Cyborg and Bionic Systems, 5, 0115.

[16] Yang, X., She, H., Lu, H., Fukuda, T., & Shen, Y. (2017). State of the art: bipedal robots for lower limb rehabilitation. Applied Sciences, 7(11), 1182.

[17] Shi, D., Zhang, W., Zhang, W., Ju, L., & Ding, X. (2021). Human-centred adaptive control of lower limb rehabilitation robot based on human–robot interaction dynamic model. Mechanism and Machine Theory, 162, 104340.

[18] Shen, Z., Zhuang, Y., Zhou, J., Gao, J., & Song, R. (2020). Design and test of admittance control with inner adaptive robust position control for a lower limb rehabilitation robot. International Journal of Control, Automation and Systems, 18(1), 134-142.

[19] Esquenazi, A., & Talaty, M. (2019). Robotics for lower limb rehabilitation. Physical Medicine and Rehabilitation Clinics, 30(2), 385-397.

[20] Farpour, H. R., Kazemi, M., Dehghanian, K. S., Moradi, M., & Farpour, S. (2021). Knowledge, Attitude, and Practice of general practitioners toward the rehabilitation field and team experts in Shiraz, Iran, in 2018. Shiraz E-Medical Journal, 22(7).

[21] Ding, W., Hu, B., Liu, H., Wang, X., & Huang, X. (2020). Human posture recognition based on multiple features and rule learning. International Journal of Machine Learning and Cybernetics, 11, 2529-2540.

[22] Han, S. H., Kim, H. G., & Choi, H. J. (2017, February). Rehabilitation posture correction using deep neural network. In 2017 IEEE international conference on big data and smart computing (BigComp) (pp. 400-402). IEEE.

[23] Bijalwan, V., Semwal, V. B., Singh, G., & Crespo, R. G. (2022). Heterogeneous computing model for post - injury walking pattern restoration and postural stability rehabilitation exercise recognition. Expert Systems, 39(6), e12706.

[24] Da Gama, A. E. F., de Menezes Chaves, T., Fallavollita, P., Figueiredo, L. S., & Teichrieb, V. (2019). Rehabilitation motion recognition based on the international biomechanical standards. Expert Systems with Applications, 116, 396-409.

[25] Byeon, Y. H., Lee, J. Y., Kim, D. H., & Kwak, K. C. (2020). Posture recognition using ensemble deep models under various home environments. Applied Sciences, 10(4), 1287.

[26] Qiu, Y., Wang, J., Jin, Z., Chen, H., Zhang, M., & Guo, L. (2022). Pose-guided matching based on deep learning for assessing quality of action on rehabilitation training. Biomedical Signal Processing and Control, 72, 103323.

[27] Florent Imbert,Eric Anquetil,Yann Soullard & Romain Tavenard. (2025). Mixture-of-experts for handwriting trajectory reconstruction from IMU sensors. Pattern Recognition111231-111231.

[28] Zolfa Anvari,Ali Mirhaghgoo & Yasin Salehi. (2025). Real-time angle estimation in IMU sensors: An adaptive Kalman filter approach with forgetting factor. Mechatronics103280-103280.

[29] Bi Xiaojun & Wang Hao. (2024). Appearance-Pose Joint Coordinates Information Collaboration Model for clothes-changing person re-identification. Expert Systems With Applications.

[30] Teng Fu & JinRong Wang. (2025). Relative controllability of neutral delay differential equations on quaternion skew field. Communications in Nonlinear Science and Numerical Simulation108557-108557.